Journal of Advanced Research 57 (2024) 93–105

Contents lists available at ScienceDirect

Journal of Advanced Research

journal homepage: www.elsevier.com/locate/jare

Original Article

The exoprotein Gbp of *Fusobacterium nucleatum* promotes THP-1 cell lipid deposition by binding to CypA and activating PI3K-AKT/MAPK/NF-κB pathways

Song Shen [a], Tianyong Sun [a], Xiangjiu Ding [b], Xiufeng Gu [a], Yushang Wang [a], Xiaomei Ma [a], Zixuan Li [a], Haiting Gao [a], Shaohua Ge [a,*], Qiang Feng [a,c,*]

[a] *Department of Human Microbiome & Periodontology & Implantology & Orthodontics, School and Hospital of Stomatology, Cheeloo College of Medicine, Shandong University & Shandong Key Laboratory of Oral Tissue Regeneration & Shandong Engineering Laboratory for Dental Materials and Oral Tissue Regeneration & Shandong Provincial Clinical Research Center for Oral Diseases, Jinan 250012, China*

[b] *Department of Vascular Surgery, General Surgery, Qilu Hospital of Shandong University, Jinan 250012, China*

[c] *State Key Laboratory of Microbial Technology, Shandong University, Qingdao 266237, China*

HIGHLIGHTS

- *F. nucleatum* was prevalent in diffuse intimal thickening as well as in plaque tissues;
- *F. nucleatum* participated in the foaming process of THP-1 cells by activating MAPK, PI3K-AKT, and NF-κB signaling cascades;
- The exoprotein of *F. nucleatum*, Gbp, promoted foam cell formation by interacting with CypA and CD147 and activating the PI3K-AKT, MAPK and NF-κB signaling pathways;
- Drug candidates targeting PI3K-AKT, MAPK and NF-κB signaling pathways could dramatically attenuate *F. nucleatum* induced macrophage foaming.

GRAPHICAL ABSTRACT

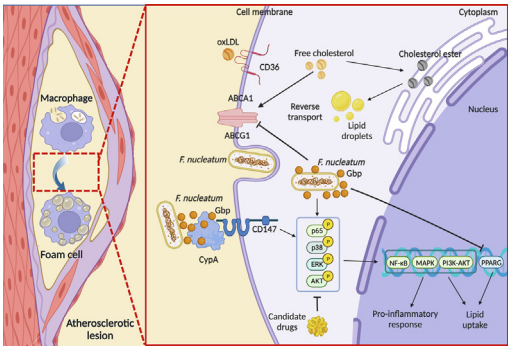

ARTICLE INFO

Article history:
Received 9 January 2023
Revised 7 April 2023
Accepted 11 April 2023
Available online 24 April 2023

Keywords:
Fusobacterium nucleatum
Lipid deposition
Gbp
CypA
RNA-seq

ABSTRACT

Introduction: Growing evidence has shown the correlation between periodontitis and atherosclerosis, while our knowledge on the pathogenesis of periodontitis-promoting atherosclerosis is far from sufficient.

Objectives: Illuminate the pathogenic effects of *Fusobacterium nucleatum* (*F. nucleatum*) on intracellular lipid deposition in THP-1-derived macrophages and elucidate the underlying pathogenic mechanism of how *F. nucleatum* promoting atherosclerosis.

Methods and results: F. nucleatum was frequently detected in different kinds of atherosclerotic plaques and its abundance was positively correlated with the proportion of macrophages. *In vitro* assays showed *F. nucleatum* could adhere to and invade THP-1 cells, and survive continuously in macrophages for 24 h. *F. nucleatum* stimulation alone could significantly promote cellular inflammation, lipid uptake and inhibit lipid outflow. The dynamic gene expression of THP-1 cells demonstrated that *F. nucleatum* could time-

Abbreviations: F. nucleatum, *Fusobacterium nucleatum*; oxLDL, oxidized low-density lipoprotein; HPLC-MS, high performance liquid chromatography-mass spectrometry; MOI, multiplicities of infection; NC, negative control; PPI, protein-protein interaction; Gbp, D-galactose-binding protein; CypA, cyclophilin A; Co-IP, co-immunoprecipitation; ELISA, enzyme-linked immunosorbent assay; siRNA, small interfering RNA.

* Corresponding authors at: No.44-1 Wenhua Road West, 250012 Jinan, Shandong, China.
E-mail addresses: shaohuage@sdu.edu.cn (S. Ge), fengqiang@sdu.edu.cn (Q. Feng).

https://doi.org/10.1016/j.jare.2023.04.007

Drug repositioning

serially induce the over-expression of multiple inflammatory related genes and activate NF-κB, MAPK and PI3K-AKT signaling pathways. The exoprotein of *F. nucleatum*, D-galactose-binding protein (Gbp), acted as one of the main pathogenic proteins to interact with the Cyclophilin A (CypA) of THP-1 cells and induced the activation of the NF- κB, MAPK and PI3K-AKT signaling pathways. Furthermore, use of six candidate drugs targeting to the key proteins in NF- κB, MAPK and PI3K-AKT pathways could dramatically decrease *F. nucleatum* induced inflammation and lipid deposition in THP-1 cells.

Conclusions: This study suggests that the periodontal pathogen *F. nucleatum* can activate macrophage PI3K-AKT/MAPK/NF-κB signal pathways, promotes inflammation, enhances cholesterol uptake, reduces lipid excretion, and promotes lipid deposition, which may be one of its main strategies promoting the development of atherosclerosis.

Introduction

Periodontitis is a prevalent oral inflammatory disease caused by the colonization of Gram-negative pathogens around teeth [1]. The periodontal pathogens can invade the blood vessel, transplant and colonize in specific tissues and organs to affect the overall health of the human body [2]. At present, growing studies suggest that periodontitis is an important risk factor for atherosclerosis [3-5]. Four underlying mechanisms link periodontitis with atherosclerosis: (1) oral pathogens invade the blood vessel and induce low-level bacteremia; (2) bacterial toxins produced by oral pathogens initiate inflammation in the blood vessel; (3) periodontal inflammatory mediators are released into bloodstream, which leads to systemic inflammation; (4) the interplay between host and particular oral pathogen components activates the autoimmunity to host proteins [6].

Fusobacterium nucleatum (*F. nucleatum*), one of the keystone pathogens in periodontitis, is widely distributed in the mouth and intestine of the human body, and has attracted wide attention in recent years [7]. Studies have shown that it can migrate from the oral cavity to colonize multiple human tissues and organs and cause a series of systemic diseases, such as colon cancer, adverse pregnancy outcomes, and rheumatoid arthritis [8]. *F. nucleatum* has been proven to be closely relevant to atherosclerosis. This is because it could be frequently detected in atherosclerotic plaques and its abundance was positively correlated with the severity of this disease [9,10]. *F. nucleatum* infection can reduce the expression of platelet endothelial cell adhesion molecule-1 (PECAM-1) and induce the death of endothelial cells [11]. The heat-shock protein GroEL of *F. nucleatum* could induce the expression of chemokines, such as interleukin (IL)-8 and E-selectin in human microvascular endothelial cells [12].

Current studies of *F. nucleatum* on atherosclerosis are mainly focused on vascular endothelial damage, while few concentrate on its pathogenic effects on the main component of atherosclerotic plaques, namely foam cells [13,14]. Mainly derived from macrophages, foam cells are triggered by uncontrolled lipid uptake and handling, as well as the impairment of cholesterol transport, which accumulates excess cholesterol from oxidized low-density lipoprotein (oxLDL) particles [15]. In this process, scavenger receptors on the surface of macrophages, such as cluster of differentiation 36 (CD36), are overexpressed and enhance oxLDL uptake [16]. Cholesterol transporters like adenosine triphosphate (ATP)-binding cassette transporter G1 and A1 (ABCG1 and ABCA1) are down-regulated and thereby reduce cholesterol outflow, which accelerates cholesterol deposition and macrophage foaming. A study showed that *F. nucleatum* speeded up macrophage foaming by the overexpression of miRNAs 155, 146a, and 23b, which lead to aberrant pro-inflammatory reactions and lipid metabolism [17]. As key sentinel cells, macrophages are an important target for abnormal lipid metabolism caused by exogenous bacterial stimuli [18] and plays a critical role in the elimination of microorganisms in the blood vessel [19].

Therefore, elucidating the pathogenesis of how *F. nucleatum* promotes macrophage foaming is essential to addressing why periodontitis contributes to the development of atherosclerosis. In this study, the effects of *F. nucleatum* on atherosclerosis were explored by analyzing the lipid metabolism and the genes/proteins expressing abnormalities in THP-1 cells. The time-series RNA-seq was applied to present the continuous alteration of gene expression in THP-1 cells with/without the stimulation of *F. nucleatum*. High performance liquid chromatography (HPLC)-mass spectrometry (MS) analysis was performed on the toxic protein of *F. nucleatum* and its host receptors to reveal the main strategy of *F. nucleatum* promoting macrophage foaming. Drug repositioning analysis was applied to select candidate chemicals to validate the main pathways and proteins through which *F. nucleatum* induces macrophage foaming.

Materials and methods

Detailed methodology is available in Supplementary Material.

Results

Frequent detection of F. Nucleatum in different kinds of atherosclerotic plaques

The RNA-seq data of atherosclerotic lesion samples from the GEO database with accession No. GSE104140 were analyzed to determine the prevalence and abundance of *F. nucleatum* in atherosclerotic plaques. It was found that *F. nucleatum* was prevalent in diffuse intimal thickening, fibroatheroma with calcification, and non-calcified fibroatheroma samples (Fig. 1A). Genes co-expressed with *F. nucleatum* were screened, and GO and KEGG enrichment analysis were performed. It was discovered that the abundance of *F. nucleatum* was mainly associated with the immune-related biological progress and pathways (Fig. 1B). Then, *F. nucleatum* co-expressed genes overlapped with all immune-related genes. A total of 55 genes were obtained, which were mainly enriched into cytokine-cytokine receptor interaction, lipid and atherosclerosis, PI3K-AKT and MAPK signaling pathway, *etc* (Fig. 1C-D).

GSE120521 dataset was downloaded and analyzed by the same procedure to verify the above results. The results showed that *F. nucleatum* was prevalent in both stable and unstable plaques. Besides, *F. nucleatum*-related genes also mainly belonged to immune-response biological progress and pathways, such as a response to lipopolysaccharide and the MAPK signaling pathway (Fig. 1E-H). Prostaglandin E receptor-1 (*PTGER-1*) associated with the inflammatory responses to pathogen infection [20], exhibited

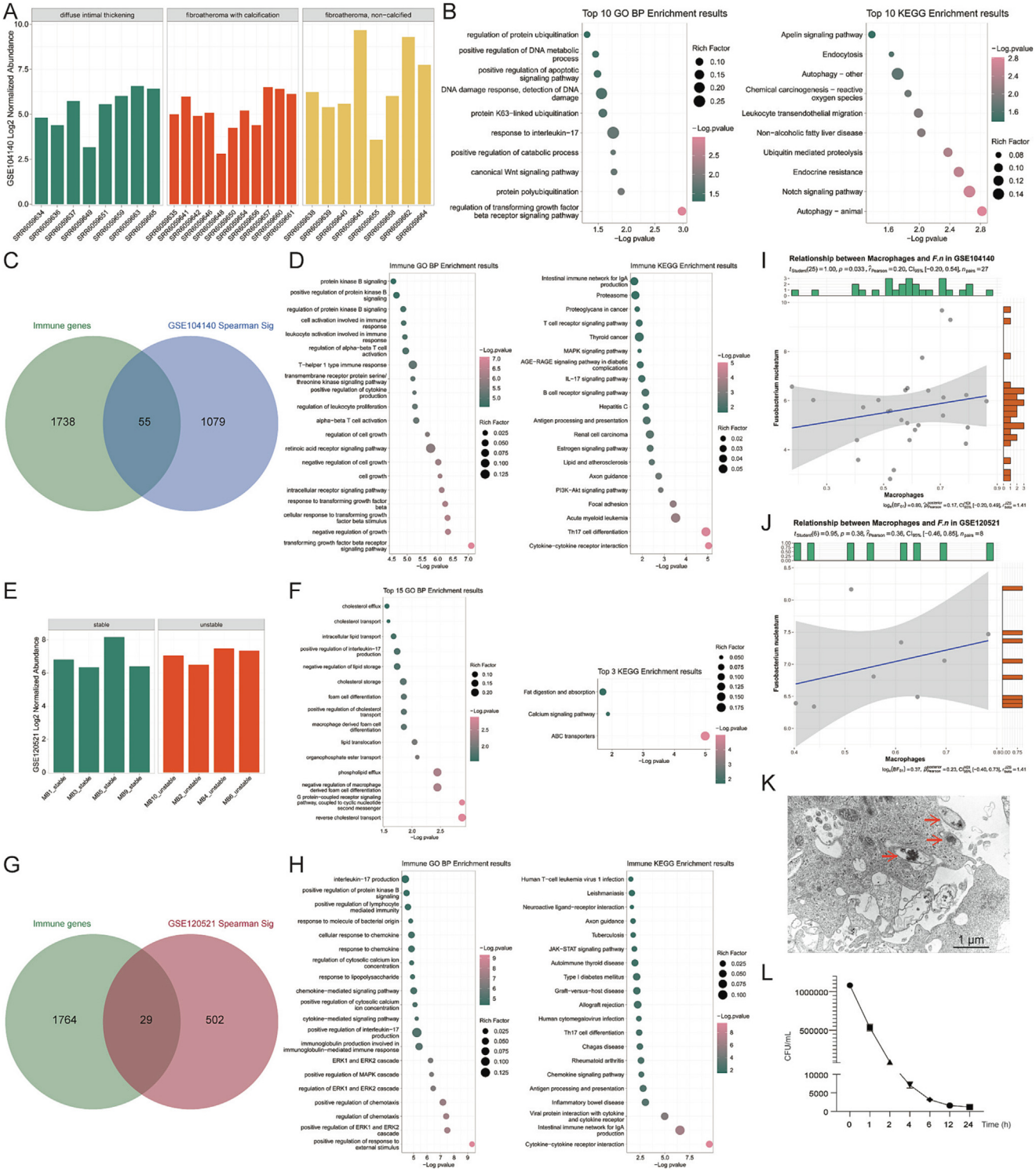

Fig. 1. The occurrence of *F. nucleatum* in different kinds of atherosclerosis plaques and its correlation with immune genes and cells. **(A)** The abundance of *F. nucleatum* in atherosclerotic lesion samples in GSE104140 dataset. **(B)** The biological processes of the genes correlated with the abundance of *F. nucleatum* in GSE104140 dataset. **(C)** Venn diagram of *F. nucleatum* co-expressing genes and all immune-related genes in GSE104140 dataset. **(D)** Functional annotation of *F. nucleatum* correlated immune genes in GSE104140 dataset. **(E)** The abundance of *F. nucleatum* in atherosclerotic lesion samples in GSE120521 dataset. **(F)** The biological processes of the genes correlated with the abundance of *F. nucleatum* in GSE120521 dataset. **(G)** Venn diagram of *F. nucleatum* co-expressing genes and all immune-related genes in GSE120521 dataset. **(H)** Functional annotation of *F. nucleatum* correlated immune genes in GSE120521 dataset. **(I)** Correlation between the proportion of macrophages and the abundance of *F. nucleatum* in GSE104140 dataset. **(J)** Correlation between the proportion of macrophages and the abundance of *F. nucleatum* in GSE120521 dataset. **(K)** TEM images of *F. nucleatum*-invading THP-1 cells (scale bar 1 μm). **(L)** The number of internalized *F. nucleatum* incubating with THP-1 cells for 0, 1, 2, 4, 6, 12, and 24 h.

a positive correlation with the abundance of *F. nucleatum* in both datasets (Figure S1A-B). CIBERSORTx was used to calculate the composition and proportion of immune cells in both datasets. It was found that macrophages occupied the highest proportion among all types of immune cells (Figure S1C-E), whose proportion was positively correlated with the abundance of *F. nucleatum*

(Fig. 1I-J). The above results implied that *F. nucleatum* may interact with immune-related genes and macrophages to contribute to the development of atherosclerosis.

F. nucleatum was used to infect macrophages. It was found that long shuttle-shaped *F. nucleatum* could not only adhere to the surface of THP-1 cells but also be present in the interior of THP-1 cells (Fig. 1K). Gentamicin protection assays at 0, 1, 2, 4, 6, 12, and 24 h showed that *F. nucleatum* could survive continuously in macrophages for up to 24 h (Fig. 1L). This indicates that macrophages cannot timely eliminate this pathogenic bacterium, which might be an important prerequisite for its pathogenicity in the human body.

Promotion of intracellular lipid accumulation by F. Nucleatum through altering the expression of lipid metabolism genes

THP-1 cells were stimulated with different multiplicities of infection (MOIs) of *F. nucleatum*, and the number of apoptotic cells accumulated with the increase of MOI (Fig. 2A). THP-1 cells were more pronounced to apoptosis at MOI $>$ 50 ($P < 0.0001$). Therefore, an MOI of 50 was chosen for the subsequent treatment in *F. nucleatum* stimulated group (*F. nucleatum* group), and *F. nucleatum* + oxLDL stimulated group (*F. nucleatum* + oxLDL group). In addition, we set up a negative control (NC) group and a positive control group, oxLDL stimulated group (oxLDL group), to compare the effects of *F. nucleatum* on macrophage foaming. More details can be found in **Material and Methods**.

The accumulation of intracellular lipids is a crucial index for the formation of foam cells. THP-1 cells were stimulated with *F. nucleatum*, oxLDL, or both for 24 h, and the lipid deposition among four groups was compared by Oil Red O staining. Compared with the NC group, the stimulation of macrophages with *F. nucleatum* alone (*F. nucleatum* group) resulted in a similar level of lipid deposition as oxLDL, while lipid deposition in *F. nucleatum* + oxLDL group far exceeded that of a single stimulus (Fig. 2B). Similarly, intracellular levels of total cholesterol ($P < 0.0001$), free cholesterol ($P < 0.0001$), and cholesteryl esters ($P < 0.01$) increased significantly after *F. nucleatum* stimulation alone (Fig. 2C). These indicators in the *F. nucleatum* + oxLDL group dramatically increased compared with any single stimulus. In additon, the morphology of THP-1 cells stimulated with *F. nucleatum* changed from the initial oval to an irregular shape with the extension of longer pseudopods (Fig. 2B).

RT-qPCR was utilized to examine the expression of genes associated with inflammation and lipid metabolism. As shown in Fig. 2D, compared to NC and oxLDL groups, *F. nucleatum* stimulation significantly promoted the expression of inflammation-related genes, such as *IL1β* ($P < 0.0001$), *IL6* ($P < 0.0001$), and matrix metallopeptidase 9 (*MMP9*) ($P < 0.0001$). *F. nucleatum* stimulation up-regulated the expression of *CD36* ($P < 0.0001$), which was bound up with cholesterol uptake and decreased the expression of cholesterol efflux-related genes, such as recombinant liver $\times$ receptor (*LXR*) ($P < 0.0001$), *ABCG1* ($P < 0.0001$), *ABCA1* ($P < 0.0001$), and peroxisome proliferator-activated receptor gamma (*PPARG*) ($P < 0.0001$). This gave rise to cholesterol accumulation in THP-1 cells. These results suggested that *F. nucleatum*, an independent factor, can promote lipid deposition and the formation of foam cells by altering the expression of inflammatory and lipid metabolism genes.

Time-series gene expression induced by F. Nucleatum in THP-1 cells

A time-series RNA-seq analysis was made of THP-1 cells at 2, 6, 12, 24, and 48 h to clarify the dynamics of gene expression during the stimulation of *F. nucleatum* or oxLDL. Firstly, maSigPro was used for independently identifying genes with significantly different expression profiles over time after stimulation with oxLDL, *F. nucleatum* or both based on quadratic regression models. As shown in Fig. 3A, three stimulation groups had a series of altered expressing genes compared with the NC group. Among them, the oxLDL group had 1083 differentially expressed genes (DEGs), while *F. nucleatum* and *F. nucleatum* + oxLDL groups had 4326 and 4790 DEGs, respectively, which differed from the NC group. Of note, DEGs in *F. nucleatum* and *F. nucleatum* + oxLDL groups were similar, with 4083 genes being the same (Table S1).

The time-series expression pattern of these genes in the *F. nucleatum* group was analyzed, and the genes with similar expression patterns were classified into one cluster. The results indicated that the stimulation of *F. nucleatum* alone could induce nine different kinds of gene expression patterns (an orange curve). The patterns of those genes in NC, oxLDL and *F. nucleatum* + oxLDL groups were also presented with green, red and blue curves, respectively (Fig. 3B). Of the nine clusters, the abundance and pattern of *F. nucleatum* and *F. nucleatum* + oxLDL groups were consistent, while those of NC and oxLDL groups were similar.

Next, the genes enriched in each cluster were annotated to GO and KEGG databases and the main affected biological processes or pathways were obtained. The results showed that genes in the same cluster could be categorized into the same or similar functional units (Table S2). Lipid accumulation and inflammatory response induced by *F. nucleatum* stimulation were the focus of this study. Thus, it was found that cluster 2 consisting of 412 genes which were rapidly up-regulated after *F. nucleatum* stimulation but dramatically decreased 12 h later had a relationship with acute immune inflammatory responses, mainly activated MAPK, NF-κB signaling pathways (Fig. 3C). Cluster 3 showed a significant down-regulation within 6 h of *F. nucleatum* stimulation while recovering gradually with the duration of *F. nucleatum* stimulation. It was mainly involved in lipid transport and localization, and activated vascular endothelial growth factor (VEGF) and rhoptry-associated protein 1 (Rap1) signaling pathways (Fig. 3D). Cluster 5 dramatically increased and reached the plateau within 6 h of *F. nucleatum* stimulation, which was enriched in pathways related to inflammatory responses and biological processes, such as MAPK, PI3K-AKT, and atherosclerosis-related pathways (Fig. 3E). The functional annotation results of the other six gene clusters were displayed in Table S2.

As shown in Fig. 2D, inflammation and intracellular lipid accumulation-related genes experienced dramatic changes under the stimulation of *F. nucleatum* or *F. nucleatum* + oxLDL. Nevertheless, a group of "non-cononical" genes may still get involved in this process. Taking advantage of the RNA-seq data of multiple time points among four groups, we used the classical inflammatory and lipid accumulation-related genes as a "bait" to find out the genes with similar expressing tendencies, which may have the same or similar functions. Mfuzz was applied to identify gene clusters with time-series dynamic patterns in each of the four groups, respectively (Figure S2). As shown in Figure S3, genes with similar expression patterns of *IL1β* and *IL6* among four groups were mainly annotated to inflammation-related pathways. However, genes with similar expression patterns of *ABCG1* and *PPARG* were mainly annotated to lipid transport and metabolism pathways, which indicated that genes with similar time-series expression patterns may have similar functions. Venn diagram showed that the dual adapter for phosphotyrosine and 3-phosphoinositides 1 (*DAPP1*), nuclear receptor co-activator protein 7 (*NCOA7*), activating transcription factor 5 (*ATF5*), phosphodiesterase 4B (*PDE4B*), and serpin family B member 8 (*SERPINB8*) had the same expression pattern with *IL1β* among the four groups (Figure S3A). Of which, *DAPP1* is a pivotal gene associated with abnormal endothelial function in early coronary atherosclerosis and is involved in the biological processes related to inflammation [21]. *NCOA7* promotes the

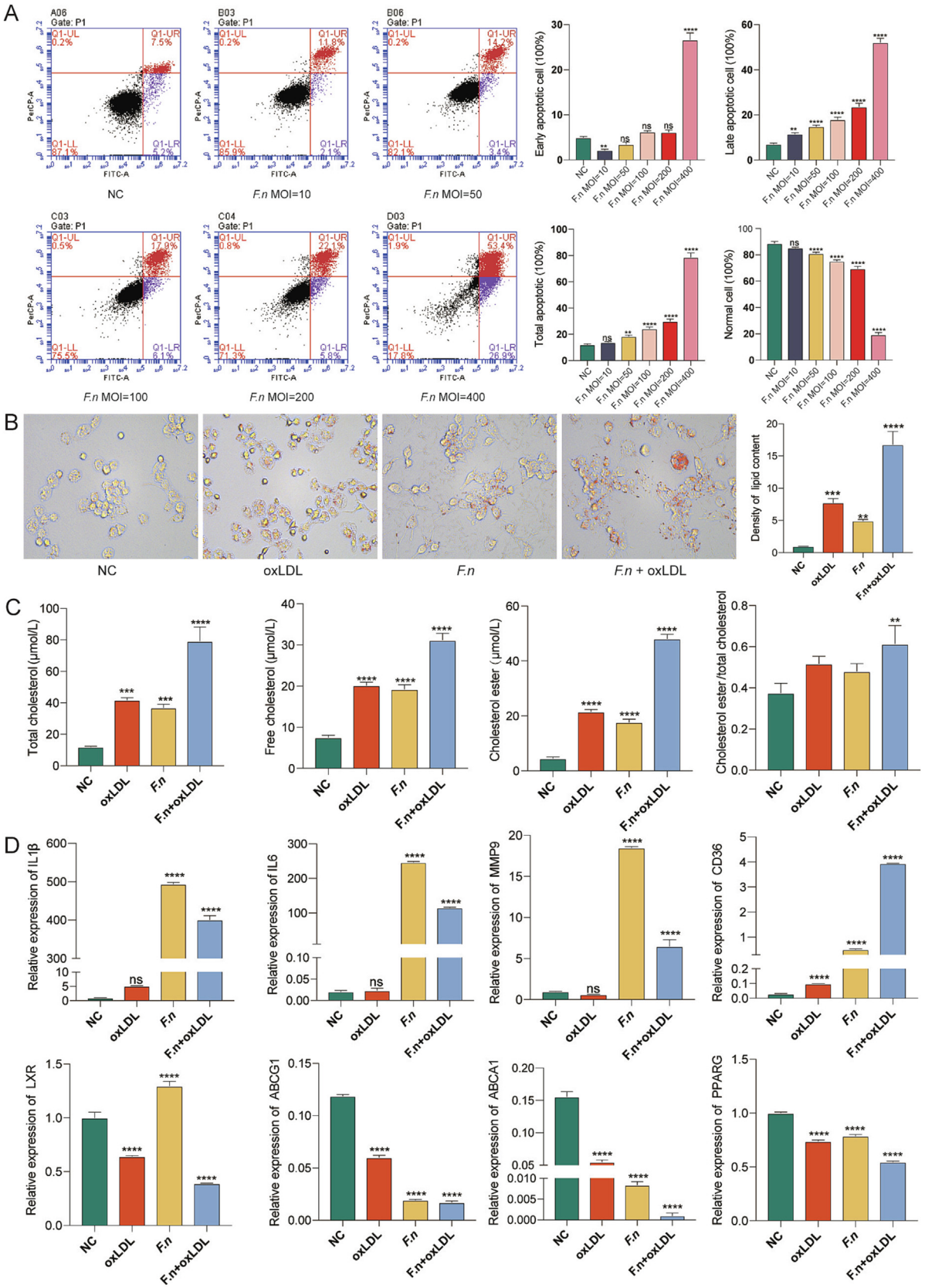

Fig. 2. The pathogenic effects of *F. nucleatum* on THP-1 cells. **(A)** Apoptosis of THP-1 cells induced by different MOIs of *F. nucleatum* stimulation. **(B)** Oil red O staining image of THP-1 cells. **(C)** Total cholesterol, free cholesterol, and cholesterol esters of THP-1 cells. **(D)** mRNA expression of *IL1β*, *IL6*, *MMP9*, *CD36*, *LXR*, *ABCG1*, *ABCA1* and *PPARG* in different groups of THP-1 cells. $^{**}P < 0.01$, $^{***}P < 0.001$ and $^{****}P < 0.0001$. (For interpretation of the references to colour in this figure legend, the reader is referred to the web version of this article.)

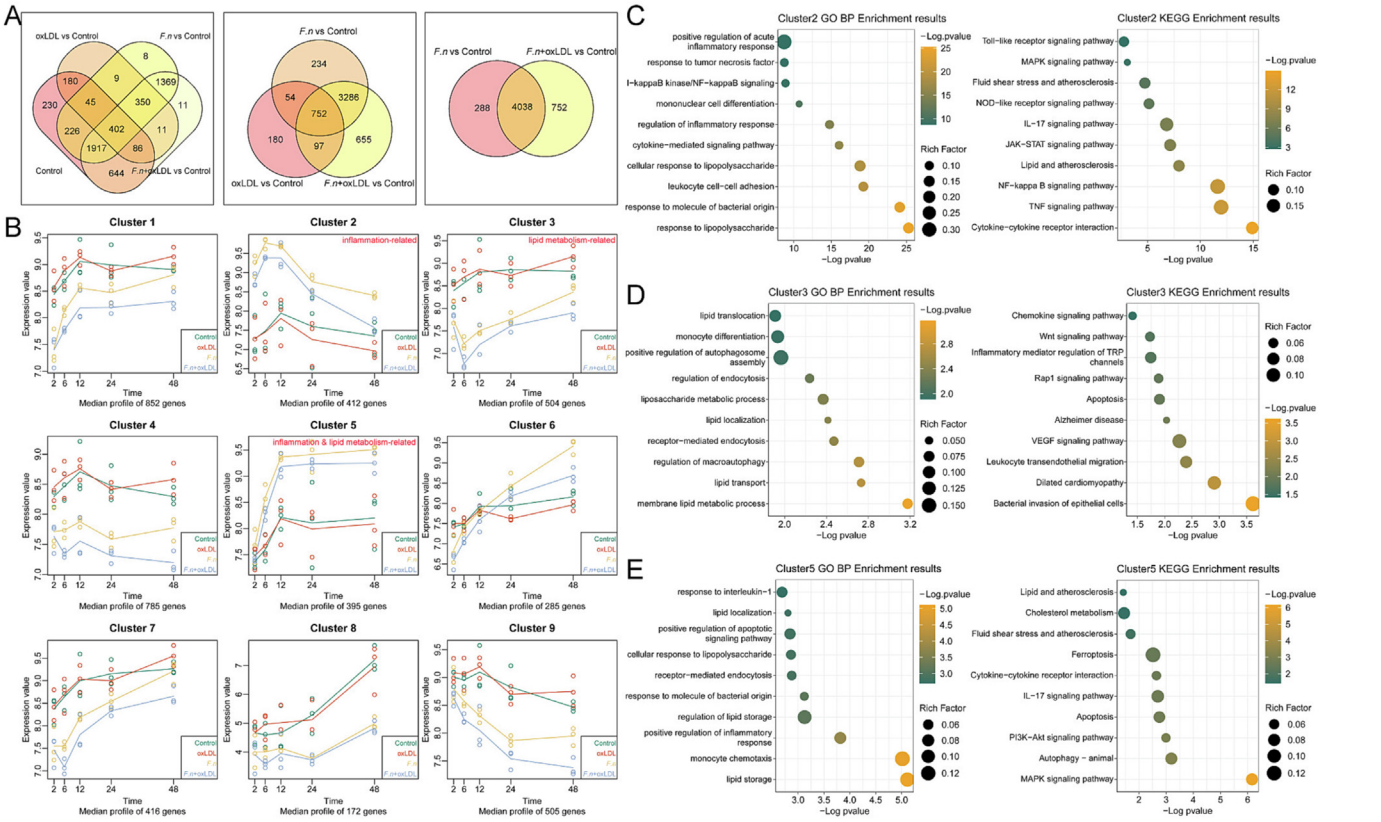

Fig. 3. Dynamics of gene-activating process of NC, oxLDL, *F. nucleatum* and *F. nucleatum* + oxLDL groups of THP-1 cells. **(A)** Venn diagrams of overlapping DEGs among different groups. **(B)** Gene clusters with different pattern in response to *F. nucleatum* stimulation and the trends in other three groups. **(C-E)** GOs and KEGG pathways annotated by genes of cluster 2, 3 and 5.

expression of inflammation related cytokines such as *IL1β* and *IL6* [22]. Meanwhile, Niemann-Pick disease C1 like intracellular cholesterol transporter 1 (*NPC1L1*), related to cholesterol homeostasis and promoted atherogenesis [23], showed the same expression trend as *ABCG1* (Figure S3B). Cleft lip and palate associated *trans*-membrane protein 1 (*CLPTM1*), associated with low-density lipoprotein cholesterol levels, shared a common pattern with *PPARG* (Figure S3C) [24]. It is worthwhile to deeply study the role and mechanism of these genes in the process of *F. nucleatum* induced macrophage foaming.

Expression of NF-κB, MAPK and PI3K-AKT signaling pathways activated by F. Nucleatum

The analysis of DEGs was performed on NC and the other three experimental groups at each time point, with a view to further investigate the genes and pathways mostly influenced by the stimulation of *F. nucleatum*. NC and *F. nucleatum* groups were compared to identify 2470, 3326, 3085, 2823, 3008 up-regulated genes and 2995, 3493, 3180, 2999, 3098 down-regulated genes at 2, 6, 12, 24, 48 h (Figure S4A). Venn plots revealed the consistent up-regulation of 412 genes and down-regulation of 287 genes in the whole process (Figure S4C). Compared with the NC group, the *F. nucleatum* + oxLDL one was found to have 291 up-regulated genes and 308 down-regulated genes after the intersection of DEGs at each time point (Figure S4B- D). In the process of *F. nucleatum* stimulation, a large number of genes was activated instantaneously and expressed continuously, which indicated that macrophages could timely sense and respond to the stimulation of pathogenic microorganisms.

To reveal the molecular bases of lipid deposition induced by *F. nucleatum* or *F. nucleatum* + oxLDL stimulation, DEGs in GO and KEGG databases were annotated, respectively. As presented in Figure S5, the genes up-regulated by *F. nucleatum* stimulation were mainly related to inflammatory response, such as NF-κB and MAPK signaling pathways, and atherosclerosis pathways (Figure S5A). In contrast, genes down-regulated by *F. nucleatum* stimulation primarily affected cell migration and metabolic processes (Figure S5B). In the *F. nucleatum* + oxLDL group, the up-regulated genes were also enriched in immune-related pathways, such as NF-κB, MAPK pathways and biological processes that affected lipids and atherosclerosis (Figure S5C), while the down-regulated genes were mainly related to cardiac and arterial developmental processes (Figure S5D). These results demonstrated that DEGs induced by *F. nucleatum* and *F. nucleatum* + oxLDL stimulation had similar functions.

To compare their similarity in the level of gene composition, a Veen diagram was drawn, and obtained DEGs at each time point of the two groups (Figure S4C-D). Recurrent DEGs were overlapped, and 240 up-regulated genes and 160 down-regulated genes at each time point of the two groups were obtained (Fig. 4-A-B). Heat-map analysis revealed that overlapping DEGs had a consistent time-series expression pattern in two groups (Fig. 4C). GO and KEGG analyses showed that the up-regulated DEGs were abundant in NF-κB, MAPK and PI3K-AKT signaling pathways, and involved in the biological process of the immune response, iron death, autophagy and tumorigenesis, *etc* (Fig. 4D-E).

Moreover, these overlapping DEGs of two groups were put into the STRING database for protein–protein interaction (PPI) analysis and 293 edges and 172 nodes were identified. The up-regulated genes and important nodes were strongly associated with

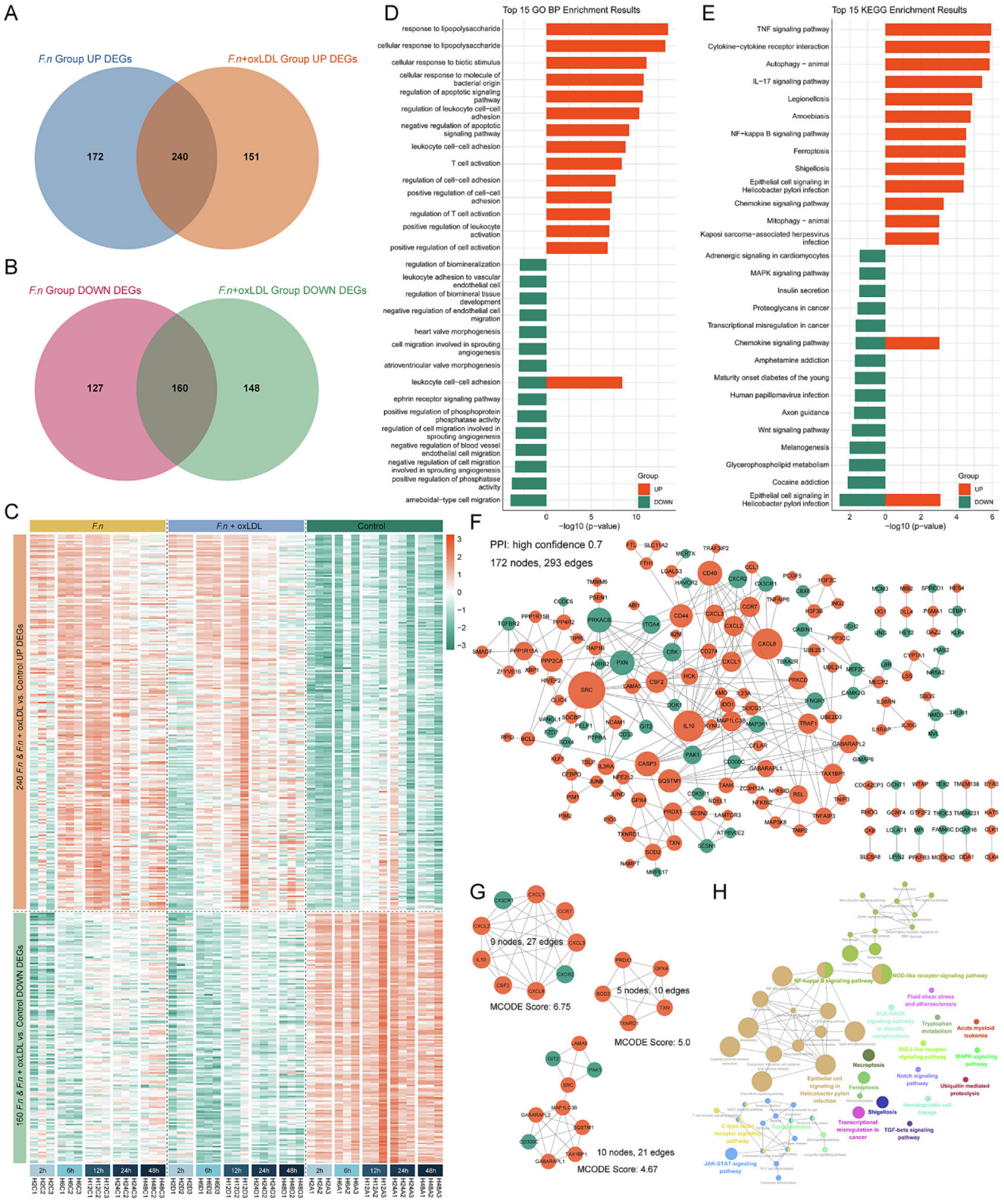

Fig. 4. DEGs and their functions shared by *F. nucleatum* and *F. nucleatum* + oxLDL groups at all time points. **(A, B)** Venn diagram of up-regulated/down-regulated genes in *F. nucleatum* and *F. nucleatum* + oxLDL groups among all time points. **(C)** Time serial expression of the overlapping DEGs in NC, *F. nucleatum* and *F. nucleatum* + oxLDL groups. **(D)** Top 15 enriched GO biological processes of the overlapping DEGs. **(E)** Top 15 enriched KEGG pathways of the overlapping DEGs. **(F)** PPI network of the overlapping DEGs (high confidence 0.7). **(G)** The significant modules obtained from PPI network (MCODE:6.75, 5.0, 4,67). **(H)** KEGG pathways of potential targets. Up-regulation marked in red; Down-regulation marked in green. (For interpretation of the references to colour in this figure legend, the reader is referred to the web version of this article.)

immunological processes (such as *CXCL8*, *IL10* and *SRC*) (Fig. 4F). Cytoscape showed that the highest scoring sub-networks were in connection with immune inflammatory response, oxidative stress, autophagy and ubiquitination, respectively (Fig. 4G). The KEGG analysis of 172 nodes using ClueGO showed that NF-κB, MAPK and PI3K-AKT and other pathways related to immune inflamma-

tion, tumor formation, atherosclerosis and ferroptosis were significantly enriched in these overlapping DEGs (Fig. 4H). These results indicated that NF-κB, MAPK and PI3K-AKT are the major activating signal pathways of *F. nucleatum* stimulating macrophages.

The application of ssGSEA analysis in all RNA-seq data helped assess the expression characteristics of NF-κB, MAPK, and PI3K-AKT pathways at each time point of four groups. The results showed that these three pathways were expressed throughout the experimental period (48 h) (Fig. 5A), and activated by *F. nucleatum* stimulation more pronouncedly (Fig. 5B). Next, Pearson correlation analysis identified the genes co-expressed with NF-κB, MAPK, and PI3K-AKT pathways and annotated in GO and KEGG databases. The results showed that, other pathways related to lipid metabolisms and inflammation, such as PPAR, IL-17, and toll-like receptor signaling pathways, were also markedly activated during *F. nucleatum* stimulation in addition to these three pathways (Fig. 5C-E).

Activation of NF-κB, MAPK, and PI3K-AKT pathways by the interaction between D-galactose-binding protein (Gbp) and Cyclophilin A (CypA)

Identifying the effector of *F. nucleatum* on THP-1 cells is an important step for further deciphering the pathogenesis of this pathogenic bacterium. A biotin pull-down assay and HLPC-MS analysis were performed to identify eight candidate proteins from *F. nucleatum* that may interact with host proteins (Table S3). Uniprot database showed that Gbp was primarily located in the periplasm of bacterial cells. Periplasmic space protein is the first communicating medium for pathogenic bacteria and host cells [25], which makes it easier to be recognized by macrophage. Hence, Gbp was selected as a candidate protein for subsequent experiments.

As shown in Figure S6a and S6b, the expression plasmid of Gbp was successfully constructed, and the Gbp protein in *Escherichia coli* (*E. coli*), which comprises 341 amino acid residues with a predicted molecular mass of 36.4 kDa, was purified. Next, the cells with different concentrations (0, 0.001, 0.01, 0.05, 0.1, 0.5, 1 mg/mL) of Gbp were stimulated. It was found that Gbp had no impact on cell viability at 0.1 mg/mL (Figure S6C), which was selected for subsequent studies. BODIPY staining was applied to present intracellular lipid droplets. It was noticed that Gbp could significantly increase the content of lipid droplets in THP-1 cells ($P < 0.0001$) (Fig. 6A-B). Meanwhile, Gbp dramatically promoted the expression of inflammation-related genes (*IL1β*, *IL6*, *MMP9*) ($P < 0.0001$), lipid uptake-related genes (*CD36*) ($P < 0.0001$) and inhibited the expression of lipid efflux-related

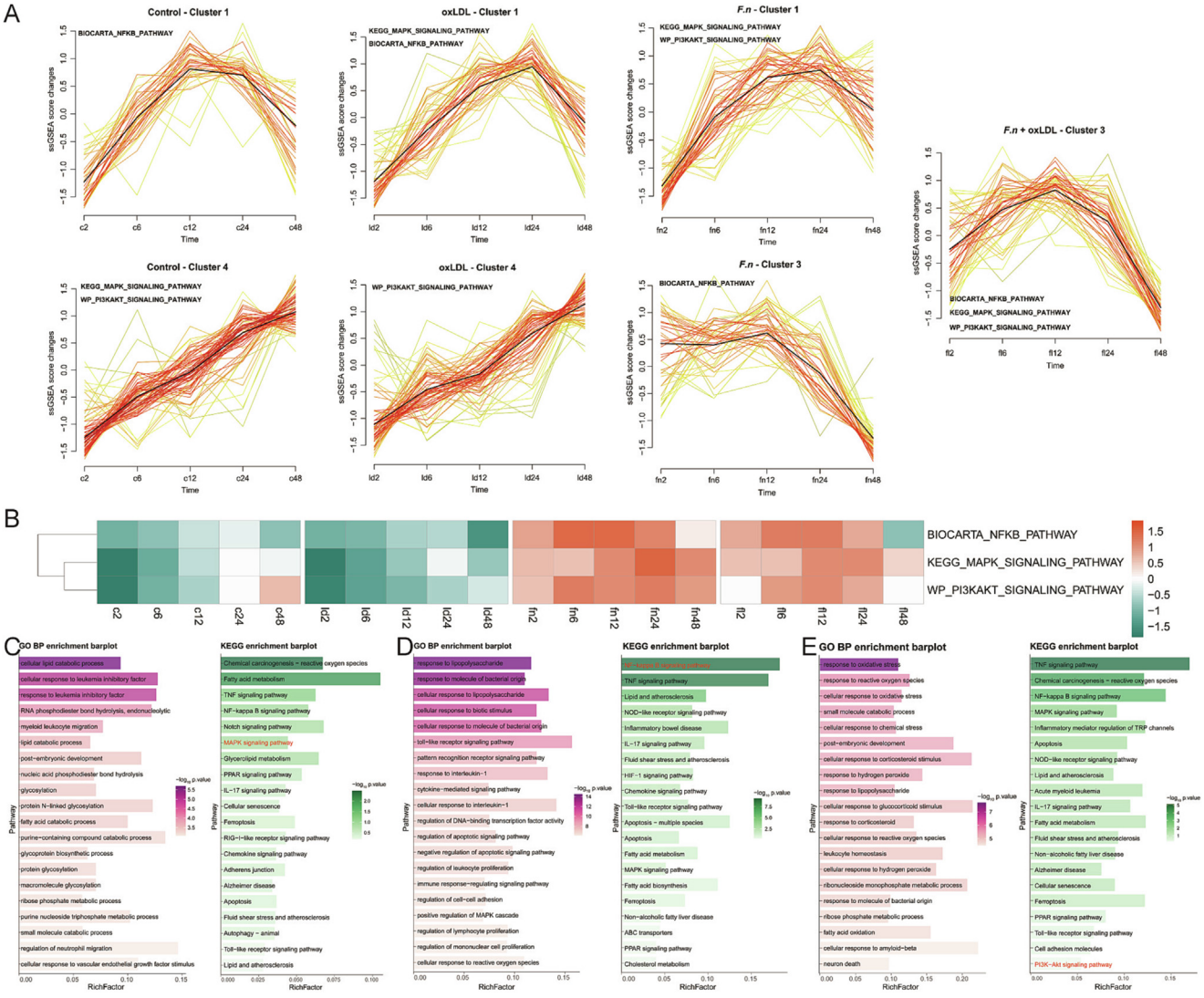

Fig. 5. The key pathways dynamically activated in different groups. **(A)** Dynamics of MAPK, PI3K-AKT, NF-κB pathways in different groups. **(B)** Abundance of the MAPK, PI3K-AKT, NF-κB pathways on 2, 6, 12, 24, and 48 h in four groups. **(C-E)** GO and KEGG annotation of MAPK, PI3K-AKT and NF-κB pathway related genes.

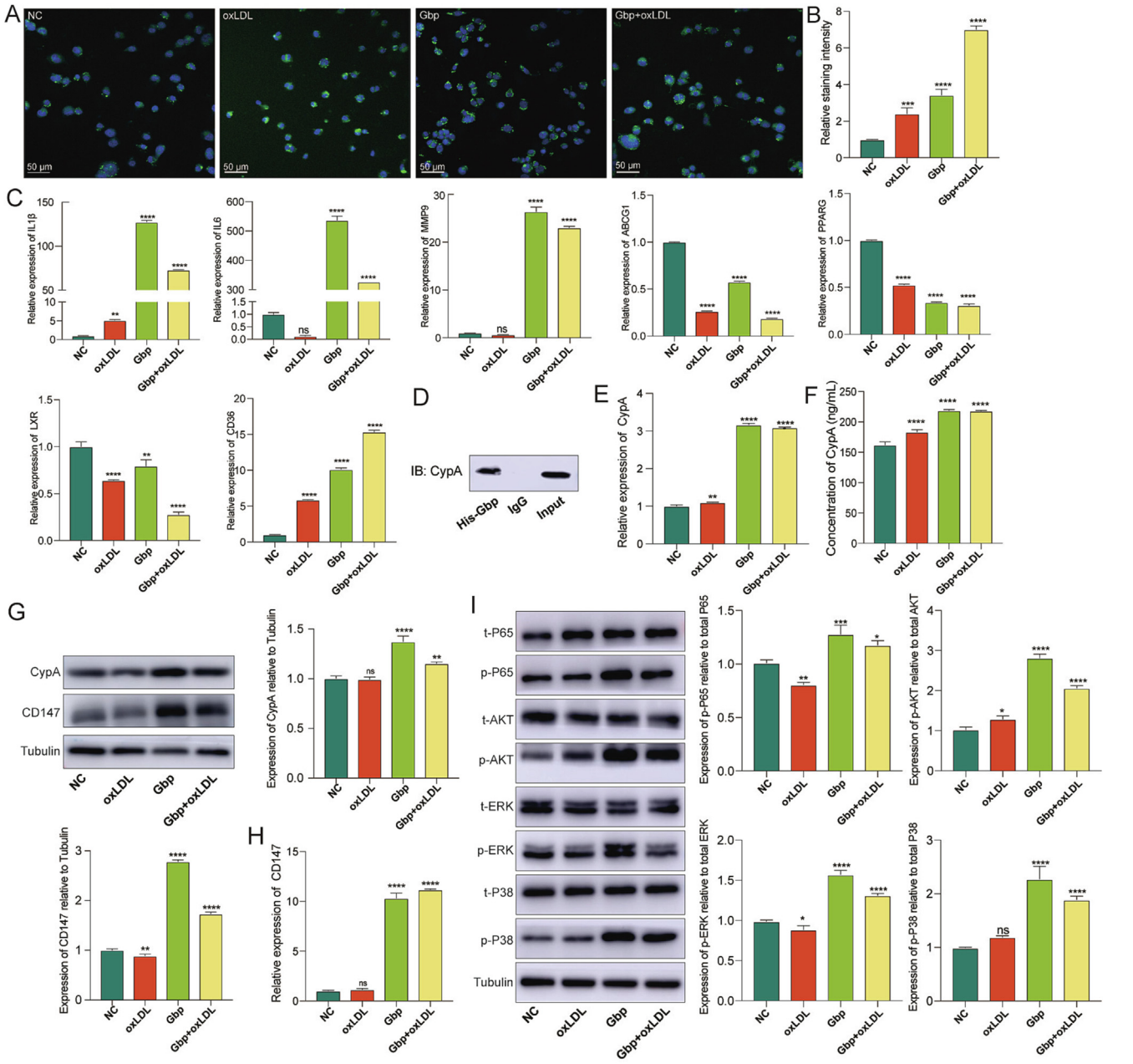

Fig. 6. The pathogenic effects of Gbp on THP-1 cells. **(A, B)** Fluorescence image and quantification of BODIPY staining (scale bar 50 μm). **(C)** The expression of *IL-1β*, *IL-6*, *MMP9*, *CD36*, *PPARG*, *ABCG1* and *LXR*. **(D)** Co-IP analysis of Gbp and CypA. **(E)** mRNA expression of *CypA*. **(F)** ELISA test of CypA. **(G)** The abundance CypA and CD147. **(H)** mRNA level of *CD147*. **(I)** The phosphorylation of P65, AKT, ERK, and P38. $^{*}P < 0.05$, $^{**}P < 0.01$, $^{***}P < 0.001$ and $^{****}P < 0.0001$.

genes (*ABCG1, PPARG, LXR*) ($P < 0.0001$) (Fig. 6C). These results suggested that Gbp is an important effector of *F. nucleatum* to promote lipid deposition of THP-1 cells.

Next, the corresponding host proteins that could interact with Gbp were identified. His-tagged Gbp was used to perform a His pull-down assay with THP-1 proteins. HLPC-MS analysis identified eight candidate proteins that may interact with His-Gbp (Table S4). Among these candidates, CypA was successfully validated to interact with Gbp by a co-immunoprecipitation (Co-IP) assay (Fig. 6D). RT-qPCR showed that Gbp promoted the expression of *CypA* to a large extent (Fig. 6E). Previous studies showed that CypA could act as a receptor inside cells [26], or in special cases, secreted extracellularly to participate in the biological processes of the inflammatory response, vascular remodeling and apoptosis [27]. Whether Gbp stimulation could induce the overexpression of CypA within cells or promote its exocrine secretion was analyzed. An enzyme-linked immunosorbent assay (ELISA) and Western blotting showed that Gbp greatly increased the abundance of intracellular and extracellular CypA simultaneously (Fig. 6F-G). Extracellular CypA can bind to the membrane receptor CD147 on monocytes, to activate ERK and NF-κB signaling pathways, and participate in the transduction of multiple signal [28-30]. The results of this study showed that CD147 saw a dramatic increase on both mRNA and protein levels under the stimulation of Gbp (Fig. 6G-H). The expression of the genes in PI3K-AKT, MAPK, and NF-κB signaling pathways were examined as CD147 is the upstream protein of these pathways. It was noted that Gbp stimulation markedly activated these signaling pathways by promoting the phosphorylation of AKT ($P < 0.0001$), ERK ($P < 0.0001$), p38 ($P < 0.0001$) and p65 ($P < 0.05$) (Fig. 6I).

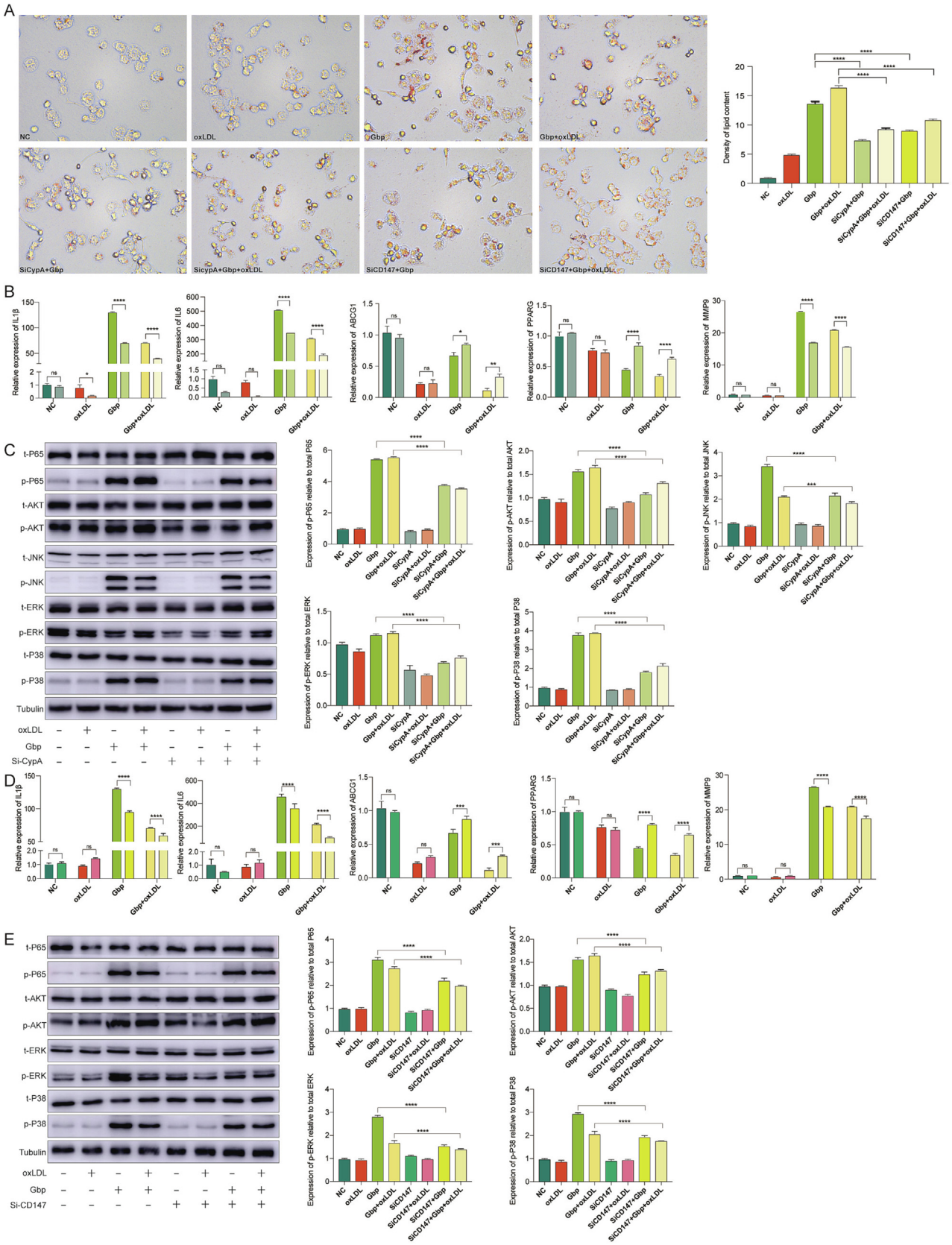

Fig. 7. Effects of CypA and CD147 on the pathogenicity of Gbp. **(A)** Oil red O staining image of THP-1 cells. **(B)** mRNA level of *IL1β*, *IL6*, *ABCG1*, *PPARG* and *MMP9* before (dark colour) and after (light colour) knockdown of CypA. **(C)** The phosphorylation of P65, AKT, JNK, ERK, and P38 before and after knockdown of CypA. **(D)** mRNA level of *IL1β*, *IL6*, *ABCG1*, *PPARG* and *MMP9* before (dark colour) and after (light colour) knockdown of CD147. **(I)** The phosphorylation of P65, AKT, ERK, and P38 before and after knockdown of CD147. $^{***}P < 0.001$ and $^{****}P < 0.0001$. (For interpretation of the references to colour in this figure legend, the reader is referred to the web version of this article.)

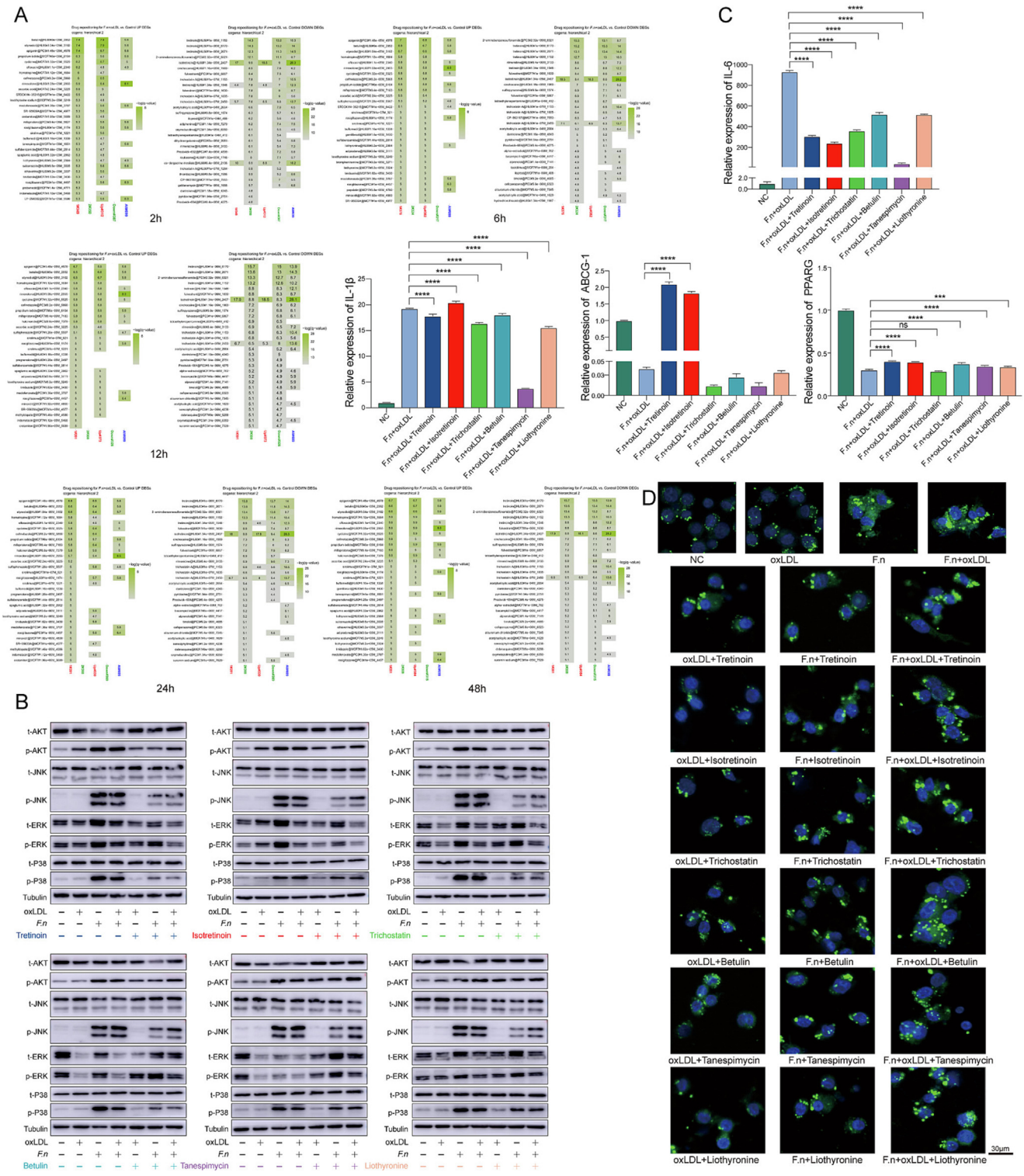

Fig. 8. Drug candidates identified to adverse *F. nucleatum* induced lipid deposition**. (A)** Computational drug repositioning analysis between NC and *F. nucleatum* + oxLDL group. **(B)** Candidate drugs attenuated the phosphorylation of AKT, JNK, ERK, and P38. **(C)** Candidate drugs attenuated the expression of IL-1β, IL-6, PPARG, and ABCG1. **(D)** BODIPY staining of THP-1 cells with *F. nucleatum* and different candidate drugs (scale bar 30 μm). $^{***}P < 0.001$ and $^{****}P < 0.0001$.

CypA was knocked down by small interfering RNA (siRNA) to further demonstrate that Gbp functioned in conjunction with CypA (Figure S6D-E). With the stimulation of Gbp, CypA knockdown dramatically reduced the formation of lipid droplets ($P < 0.0001$) (Fig. 7A), decreased the expression of inflammatory factors *IL1β* ($P < 0.0001$), *IL6* ($P < 0.0001$), *MMP9* ($P < 0.0001$), and increased the expression of lipid efflux-related genes *PPARG* ($P < 0.0001$), *ABCG1* ($P < 0.05$) (Fig. 7B). Of PI3K-AKT, MAPK, and NF-κB pathways, CypA knockdown decreased the expression of AKT ($P < 0.0001$), JNK ($P < 0.0001$), ERK ($P < 0.0001$), p38 ($P < 0.0001$) and p65 ($P < 0.0001$) (Fig. 7C). These results showed that the pathogenic effect of Gbp on THP-1 cells was exerted by its interaction with CypA.

The necessity of CD147 in Gbp-induced signaling transduction and cytological behavior changes was verified by the use of siRNA

knockdown. As shown in Fig. 7A, CD147 knockdown dramatically reduced the formation of lipid droplet ($P < 0.0001$), decreased the expression of *IL1β* ($P < 0.0001$), *IL6* ($P < 0.0001$), *MMP9* ($P < 0.0001$), and increased the expression of *PPARG* ($P < 0.001$), *ABCG1* ($P < 0.0001$) (Fig. 7D). Meanwhile CD147 knockdown suppressed the activation of PI3K-AKT, MAPK, and NF-κB pathways by reducing p-AKT ($P < 0.0001$), p-ERK ($P < 0.0001$), p-P38 ($P < 0.0001$), p-P65 ($P < 0.0001$) (Fig. 7E). These results suggested that CD147 is an important mediator for Gbp to exert pathogenic effects on THP-1 cells.

Attenuation of F. nucleatum-induced lipid deposition by drugs targeting NF-κB, MAPK, and PI3K-AKT pathways

To verify the role of NF-κB, MAPK, and PI3K-AKT pathways in lipid deposition induced by *F. nucleatum*, a drug repositioning analysis was performed based on the gene-expression pattern regulated by *F. nucleatum* stimulation, and a series of candidate therapeutic agents were identified (Fig. 8A). Targets of these drugs were retrieved by the Drug-Gene Interaction database (DGIdb) (Figure S7A) and KEGG pathway enrichment analysis (Figure S7B). Six different candidate drugs were selected, including tretinoin, isotretinoin, liothyronine, betulin, trichostatin, and tanespimycin, as they could interfere with the PI3K-AKT, MAPK and NF-κB signaling pathways (Figure S7C-F).

A CCK8 viability assay was applied to select the optimal concentration of each drug (Figure S8A). We chose drug concentrations that have no effect on cell viability for subsequent experiments, namely 10 μM of tretinoin, 10 μM of isotretinoin, 100 nM of liothyronine, 10 μM of betulin, 1 μM of trichostatin, and 100 nM of tanespimycin. Next, the effects of each candidate drug on MAPK and PI3K-AKT pathways under the stimulation of *F. nucleatum* were tested. The results showed tretinoin could impede the PI3K-AKT pathway by inhibiting the phosphorylation of AKT ($P < 0.001$), and inhibit the MAPK signaling pathway by decreasing the expression of p-JNK ($P < 0.001$), p-ERK ($P < 0.01$), and p-P38 ($P < 0.001$); isotretinoin and liothyronine could suppress MAPK pathway by reducing p-JNK ($P < 0.005$); trichostatin could attenuate the activation of MAPK *via* decreasing p-JNK ($P < 0.001$) and p-P38 ($P < 0.001$); betulin could restrain the expression of p-JNK ($P < 0.001$), p-ERK ($P < 0.05$), and p-P38 ($P < 0.001$) in MAPK pathway; while tanespimycin could repress p-ERK ($P < 0.05$), and p-P38 ($P < 0.01$) (Fig. 8B, S8B).

Inflammatory and lipid deposition related-gene analysis showed that all of these six drugs dramatically reduced the expression of inflammatory factors *IL1β* ($P < 0.001$) and *IL6* ($P < 0.001$), and all drugs except trichostatin increased the expression of *PPARG* ($P < 0.001$). Besides, tretinoin and isotretinoin enhanced the expression of *ABCG1* ($P < 0.001$) (Fig. 8C). BODIPY staining experiments intuitively demonstrated that all of these candidate drugs effectively down-regulated *F. nucleatum*-induced intracellular lipid deposition ($P < 0.001$) (Fig. 8D, S8C). These results further proved that NF-κB, MAPK, and PI3K-AKT pathways were the main mediators by which *F. nucleatum* exerted its pathogenic effects on THP-1 cells and also suggested that the great potential of these drugs to treat *F. nucleatum* induced atherosclerosis by targeting these pathways.

Discussion

Increasing evidence indicates that atherosclerosis is a chronic inflammatory disease [31]. DNA testing showed that pathogens in severe chronic periodontitis were identified in 50% of atherosclerotic plaque [32]. Similarly, it was found that *F. nucleatum* existed in all atherosclerosis lesions *via* the analysis of two public RNA-seq datasets. A study showed that *F. nucleatum* could invade host cells under aerobic conditions and survive for 48 h [33]. This study further proved that *F. nucleatum* is capable of adhering, invading and surviving in macrophages, which may be one of the main strategies for *F. nucleatum* to exert its pathogenicity.

As is known to all, macrophage-derived foam cells are associated with atherosclerosis [34]. The present study showed that *F. nucleatum* promoted macrophage foaming by increasing the expression of the lipid-uptake receptors, such as CD36 [35], and reducing the expression of cholesterol efflux-related transporter proteins ABCG1 and ABCA1 [36]. The key upstream transcription factors, PPARG and LXR [37], were also significantly down-regulated in response to *F. nucleatum* stimulation. Furthermore, it was demonstrated that *F. nucleatum* enhanced lipid deposition by activating NF-κB, MAPK, and PI3K-AKT pathways, which is the key event in the development of macrophage-derived foam cells [38,39]. Herein, the result indicated that *F. nucleatum* induced macrophage foaming by activating series of classical signaling pathways.

Moreover, a protein called Gbp was discovered in *F. nucleatum*. Involved in the active transport of glucose, galactose and mediating bacterial chemotaxis [40-42], this protein may interact with the CypA of THP-1 cells to promote inflammation and lipid deposition. Ubiquitously distributed in intracellular and extracellular space [43], CypA was first identified as a receptor for Cyclosporine A and later proved to be secreted extracellularly as well [27,44]. A previous study showed that CypA promoted the cellular uptake of LDL by enhancing the expression of scavenger receptors [45]. Likewise, this research firstly demonstrated that *F. nucleatum* exoprotein Gbp might facilitate lipid deposition through its interaction with CypA, which communicated information to CD147 to activate the PI3K-AKT, MAPK, and NF-κB signaling pathways.

Candidate drugs targeting NF-κB, MAPK, and PI3K-AKT pathways were used to verify whether the pathogenesis of *F. nucleatum* on THP-1 cells was mainly through these classical pathways. The results showed that these drugs significantly inhibited the activation of these signaling pathways, which thus reduced the level of lipid deposition. The result of this study demonstrated the main pathways by which *F. nucleatum* induced lipid deposition in macrophages, and also provided new drug candidates to treat *F. nucleatum* induced atherosclerosis.

To sum up, the present study suggests that *F. nucleatum* is involved in the process of atherosclerosis development through the activation of MAPK, PI3K-AKT, and NF-κB signaling pathways via the Gbp-CypA-CD147 complex. These results provide new knowledge on how periodontitis promotes atherosclerosis, while this may be one of the mechanisms of *F. nucleatum* promoting macrophage foaming, and there are still many potential ways to be clarified. Besides, further studies are needed to explore the therapeutic potential of targeting the Gbp-CypA-CD147 complex and its downstream signaling pathways for the prevention or treatment periodontitis associated atherosclerosis.

Compliance with ethics requirements

This study does not involve the use of human and animal subjects.

Declaration of Competing Interest

The authors declare that they have no known competing financial interests or personal relationships that could have appeared to influence the work reported in this paper.

Acknowledgements

We sincerely thank all colleagues in our laboratory for all of the kindly advices and support. We sincerely thank the foundation support of the National Natural Science Foundation of China (No. 82071122, 82270980), the National Young Scientist Support Foundation (2019), Excellent Young Scientist Foundation of Shandong Province (No. ZR202102230369), Taishan Young Scientist Project of Shandong Province, Periodontitis innovation team of Jinan City (2021GXRC021), Major Innovation Projects in Shandong Province (No. 2021SFGC0502), Oral Microbiome Innovation Team of Shandong Province (No. 2020KJK001), Shandong Province Key Research and Development Program (No. 2021ZDSYS18), Shandong Province Major Scientific and Technical Innovation Project (No. 2021SFGC0502), the Construction Engineering Special Fund of "Taishan Scholars" of Shandong Province (No. ts20190975).

Appendix A. Supplementary material

Supplementary data to this article can be found online at https://doi.org/10.1016/j.jare.2023.04.007.

References

[1] Bao J, Li L, Zhang Y, Wang M, Chen F, Ge S, et al. Periodontitis may induce gut microbiota dysbiosis via salivary microbiota. Int J Oral Sci 2022;14(1).
[2] Peng X, Cheng L, You Y, Tang C, Ren B, Li Y, et al. Oral microbiota in human systematic diseases. Int J Oral Sci 2022;14(1).
[3] Wolf D, Ley K. Immunity and inflammation in atherosclerosis. Circ Res 2019;124(2):315–27.
[4] Hansson GK, Hermansson A. The immune system in atherosclerosis. Nat Immunol 2011;12(3):204–12.
[5] Zardawi F, Gul S, Abdulkareem A, Sha A, Yates J. Association between periodontal disease and atherosclerotic cardiovascular diseases: revisited. Front Cardiovasc Med 2021;7:625579.
[6] Aarabi G, Heydecke G, Seedorf U. Roles of oral infections in the pathomechanism of atherosclerosis. Int J Mol Sci 2018;19:1978.
[7] Li B, Ge Y, Cheng L, Zeng B, Yu J, Peng X, et al. Oral bacteria colonize and compete with gut microbiota in gnotobiotic mice. Int J Oral Sci 2019;11(1).
[8] Gur C, Ibrahim Y, Isaacson B, Yamin R, Abed J, Gamliel M, et al. Binding of the Fap2 protein of Fusobacterium nucleatum to human inhibitory receptor TIGIT protects tumors from immune cell attack. Immunity 2015;42(2):344–55.
[9] Gaetti-Jardim E, Marcelino SL, Feitosa ACR, Romito GA, Avila-Campos MJ. Quantitative detection of periodontopathic bacteria in atherosclerotic plaques from coronary arteries. J Med Microbiol 2009;58:1569–75.
[10] Elkaïm R, Dahan M, Kocgozlu L, Werner S, Kanter D, Kretz JG, et al. Prevalence of periodontal pathogens in subgingival lesions, atherosclerotic plaques and healthy blood vessels: a preliminary study. J Periodontal Res 2008;43 (2):224–31.
[11] Farrugia C, Stafford GP, Gains AF, Cutts AR, Murdoch C. Fusobacterium nucleatum mediates endothelial damage and increased permeability following single species and polymicrobial infection. J Periodontol 2022;93(9):1421–33.
[12] Lee HR, Jun HK, Kim HD, Lee SH, Choi BK. Fusobacterium nucleatum GroEL induces risk factors of atherosclerosis in human microvascular endothelial cells and ApoE(-/-) mice. Mol Oral Microbiol 2012;27:109–23.
[13] Colin S, Chinetti-Gbaguidi G, Staels B. Macrophage phenotypes in atherosclerosis. Immunol Rev 2014;262(1):153–66.
[14] Sukhorukov VN, Khotina VA, Chegodaev YS, Ivanova E, Sobenin IA, Orekhov AN. Lipid metabolism in macrophages: focus on atherosclerosis. Biomedicines 2020;8(8):262.
[15] Li J, Meng Q, Fu Yu, Yu X, Ji T, Chao Y, et al. Novel insights: Dynamic foam cells derived from the macrophage in atherosclerosis. J Cell Physiol 2021;236 (9):6154–67.
[16] Chistiakov DA, Melnichenko AA, Myasoedova VA, Grechko AV, Orekhov AN. Mechanisms of foam cell formation in atherosclerosis. J Mol Med (Berl) 2017;95(11):1153–65.
[17] Zhou J, Liu L, Wu P, Zhao L, Wu Y. Fusobacterium nucleatum accelerates atherosclerosis via macrophage-driven aberrant proinflammatory response and lipid metabolism. Front Microbiol 2022;13:798685.
[18] Robichaud S, Fairman G, Vijithakumar V, Mak E, Cook DP, Pelletier AR, et al. Identification of novel lipid droplet factors that regulate lipophagy and cholesterol efflux in macrophage foam cells. Autophagy 2021;17(11):3671–89.
[19] Locati M, Curtale G, Mantovani A. Diversity, mechanisms, and significance of macrophage plasticity. Annu Rev Pathol 2020;15(1):123–47.
[20] Ribeiro-Santos FR, Silva GGd, Petean IBF, Arnez MFM, Silva LABd, Faccioli LH, et al. Periapical bone response to bacterial lipopolysaccharide is shifted upon cyclooxygenase blockage. J Appl Oral Sci 2019;27:e20180641.
[21] Qiu X, Lin J, Chen Y, Liang B, Li L. Identification of hub genes associated with abnormal endothelial function in early coronary atherosclerosis. Biochem Genet 2022;60(4):1189–204.
[22] Cho S-H, Park SY, Lee EJ, Cho YH, Park HS, Hong S-H, et al. Regulation of CYP1A1 and inflammatory cytokine by NCOA7 isoform 4 in response to dioxin induced airway inflammation. Tuberc Respir Dis (Seoul) 2015;78(2):99.
[23] Betters JL, Yu L. NPC1L1 and cholesterol transport. FEBS Lett 2010;584:2740–7.
[24] Yang T, Wei P, Pan W, Schwartz R. Integrative analysis of multi-omics data for discovering low-frequency variants associated with low-density lipoprotein cholesterol levels. Bioinformatics 2020;36(21):5223–8.
[25] Richarme G, Caldas TD. Chaperone properties of the bacterial periplasmic substrate-binding proteins. J Biol Chem 1997;272(25):15607–12.
[26] Wang G, Shen J, Sun J, et al. Cyclophilin A Maintains Glioma-Initiating Cell Stemness by Regulating Wnt/β-Catenin Signaling. Clin Cancer Res 2017;23:6640–9.
[27] Wei Y, Jinchuan Y, Yi L, Jun Wu, Zhongqun W, Cuiping W. Antiapoptotic and proapoptotic signaling of cyclophilin A in endothelial cells. Inflammation 2013;36(3):567–72.
[28] Liao Y, Peng K, Li X, Ye Y, Liu P, Zeng Y. The adhesion protein of Mycoplasma genitalium inhibits urethral epithelial cell apoptosis through CypA-CD147 activating PI3K/Akt/NF-κB pathway. Appl Microbiol Biotechnol 2022;106(19-20):6657–69.
[29] Li L, Luo D, Liao Y, Peng K, Zeng Y. Mycoplasma genitalium protein of adhesion induces inflammatory cytokines via cyclophilin A-CD147 cctivating the ERK-NF-κB pathway in human urothelial cells. Front Immunol 2020;11:2052.
[30] Pahk K, Joung C, Song HY, Kim S, Kim WK. SP-8356, a Novel inhibitor of CD147-Cyclophilin A interactions, reduces plaque progression and stabilizes vulnerable plaques in apoE-deficient mice. Int J Mol Sci 2019;21:95.
[31] Pothineni NVK, Subramany S, Kuriakose K, Shirazi LF, Romeo F, Shah PK, et al. Infections, atherosclerosis, and coronary heart disease. Eur Heart J 2017;38 (43):3195–201.
[32] Zaremba M, Górska R, Suwalski P, Kowalski J. Evaluation of the incidence of periodontitis-associated bacteria in the atherosclerotic plaque of coronary blood vessels. J Periodontol 2007;78(2):322–7.
[33] Xue Y, Xiao H, Guo S, Xu B, Liao Y, Wu Y, et al. Indoleamine 2,3-dioxygenase expression regulates the survival and proliferation of Fusobacterium nucleatum in THP-1-derived macrophages. Cell Death Dis 2018;9(3).
[34] Guerrini V, Gennaro ML. Foam cells: one size doesn't fit all. Trends Immunol 2019;40(12):1163–79.
[35] Fan J, Liu L, Liu Q, Cui Yu, Yao B, Zhang M, et al. CKIP-1 limits foam cell formation and inhibits atherosclerosis by promoting degradation of Oct-1 by REGγ. Nat Commun 2019;10(1).
[36] Koelwyn GJ, Corr EM, Erbay E, Moore KJ. Regulation of macrophage immunometabolism in atherosclerosis. Nat Immunol 2018;19(6):526–37.
[37] Yang S, Xia Y-P, Luo X-Y, Chen S-l, Li B-W, Ye Z-M, et al. Exosomal CagA derived from Helicobacter pylori-infected gastric epithelial cells induces macrophage foam cell formation and promotes atherosclerosis. J Mol Cell Cardiol 2019;135:40–51.
[38] Reustle A, Torzewski M. Role of p38 MAPK in atherosclerosis and aortic valve sclerosis. Int J Mol Sci 2018;19(12):3761.
[39] Linton MF, Babaev VR, Huang J, Linton EF, Tao H, Yancey PG. Macrophage apoptosis and efferocytosis in the pathogenesis of atherosclerosis. Circ J 2016;80(11):2259–68.
[40] Mondal SI, Mahmud Z, Elahi M, Akter A, Jewel NA, Muzahidul Islam Md, et al. Study of intra-inter species protein-protein interactions for potential drug targets identification and subsequent drug design for Escherichia coli O104:H4 C277–11. In Silico Pharmacol 2016;5(1).
[41] Borrok MJ, Kiessling LL, Forest KT. Conformational changes of glucose/galactose-binding protein illuminated by open, unliganded, and ultra-high-resolution ligand-bound structures. Protein Sci 2007;16 (6):1032–41.
[42] Kim D-Y, Son D-H, Matin A, Jung S-Y. Production of a monoclonal antibody against a galactose-binding protein of Acanthamoeba castellanii and its cytotoxicity. Parasitol Res 2021;120(11):3845–50.
[43] Song F, Zhang X, Ren X-B, Zhu P, Xu J, Wang Li, et al. Cyclophilin A (CyPA) induces chemotaxis independent of its peptidylprolyl cis-trans isomerase activity: direct binding between CyPA and the ectodomain of CD147. J Biol Chem 2011;286(10):8197–203.
[44] Yuan W, Ge H, He B. Pro-inflammatory activities induced by CyPA-EMMPRIN interaction in monocytes. Atherosclerosis 2010;213(2):415–21.
[45] Nigro P, Satoh K, O'Dell MR, Soe NN, Cui Z, Mohan A, et al. Cyclophilin A is an inflammatory mediator that promotes atherosclerosis in apolipoprotein E-deficient mice. J Exp Med 2011;208(1):53–66.